Electronic Supplementary Material (ESI) for Chemical Science.

Electronic Supplementary Information for:

Structural characterization of framework–gas interactions in the metal–organic framework Co_2(dobdc) by *in situ* single-crystal X-ray diffraction

Miguel I. Gonzalez,[a] Jarad A. Mason,[a] Eric D. Bloch,[a] Simon J. Teat,[b] Kevin J. Gagnon,[b] Gregory Y. Morrison,[b] Wendy L. Queen,[cd] and Jeffrey R. Long*[aef]

[a]Department of Chemistry, University of California, Berkeley, California, 94720-1462, USA.
[b]Advanced Light Source, Lawrence Berkeley National Laboratory, Berkeley, California, 94720, USA.
[c]The Molecular Foundry, Lawrence Berkeley National Laboratory, Berkeley, California, 94720, USA.
[d]École Polytechnique Fédérale de Lausanne (EPFL), Institut des Sciences et Ingénierie Chimiques, CH 1051 Sion, Switzerland
[e]Department of Chemical and Biomolecular Engineering, University of California, Berkeley, California, 94720-1462, USA.
[f]Materials Sciences Division, Lawrence Berkeley National Laboratory, Berkeley, California 94720, United States, 94720, USA.

Table of Contents

Supplementary Figures

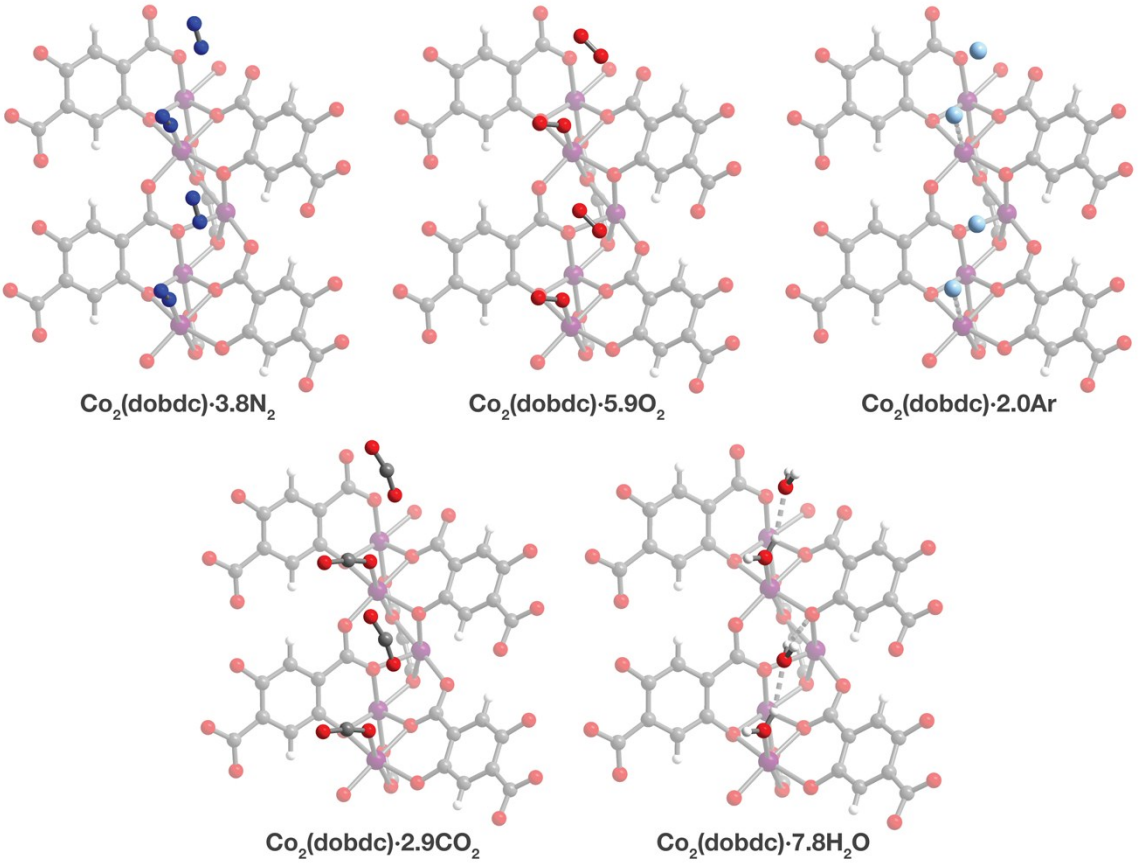

Figure S1. Comparison of the secondary binding sites in the structures of $Co_2(dobdc)\cdot 3.8N_2$ at 100 K, $Co_2(dobdc)\cdot 5.9O_2$ at 100 K, $Co_2(dobdc)\cdot 2.0Ar$ at 90 K, $Co_2(dobdc)\cdot 2.9CO_2$[1] at 150 K, and $Co_2(dobdc)\cdot 7.8H_2O$[2] at 100 K as determined by single-crystal X-ray diffraction. Purple, red, gray, blue, light blue, and white spheres represent Co, O, C, N, Ar, and H atoms, respectively. The structures of $Co_2(dobdc)\cdot 2.9CO_2$ and $Co_2(dobdc)\cdot 7.8H_2O$ have been reported previously and are shown here to facilitate comparisons.

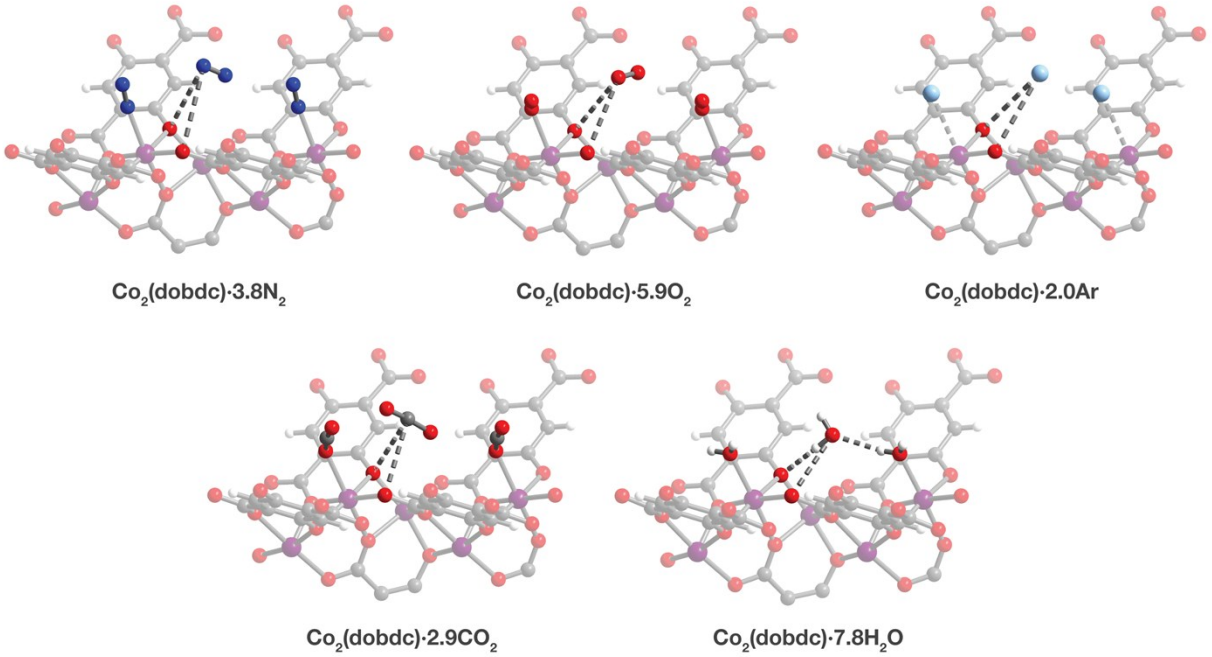

$Co_2(dobdc)\cdot 3.8N_2$		$Co_2(dobdc)\cdot 5.9O_2$		$Co_2(dobdc)\cdot 2.0Ar$		$Co_2(dobdc)\cdot 2.9CO_2$[1]		$Co_2(dobdc)\cdot 7.8H_2O$[2]	
O1···N4	3.44(2) Å	O1···O7	3.391(17) Å	O1···Ar2	3.683(16) Å	O1···C6	3.21(5) Å	O1···H5a	2.15(3) Å
O3···N4	3.66(3) Å	O3···O7	3.376(18) Å	O3···Ar2	3.767(18) Å	O3···C6	3.29(8) Å	O3···O5	3.172(4) Å

Figure S2. Selected intermolecular contacts between the phenoxide oxygen (O1) and non-bridging carboxylate oxygen (O3) of the dobdc^{4-} linkers and gases bound at secondary binding sites in the structures of $Co_2(dobdc)\cdot 3.8N_2$ at 100 K, $Co_2(dobdc)\cdot 5.9O_2$ at 100 K, $Co_2(dobdc)\cdot 2.0Ar$ at 90 K, $Co_2(dobdc)\cdot 2.9CO_2$[1] at 150 K, and $Co_2(dobdc)\cdot 7.8H_2O$[2] at 100 K as determined by single-crystal X-ray diffraction. Purple, red, gray, blue, light blue, and white spheres represent Co, O, C, N, Ar, and H atoms, respectively. The structures of $Co_2(dobdc)\cdot 2.9CO_2$ and $Co_2(dobdc)\cdot 7.8H_2O$ have been reported previously and are shown here to facilitate comparisons.

Thermal ellipsoid plots and crystallographic tables

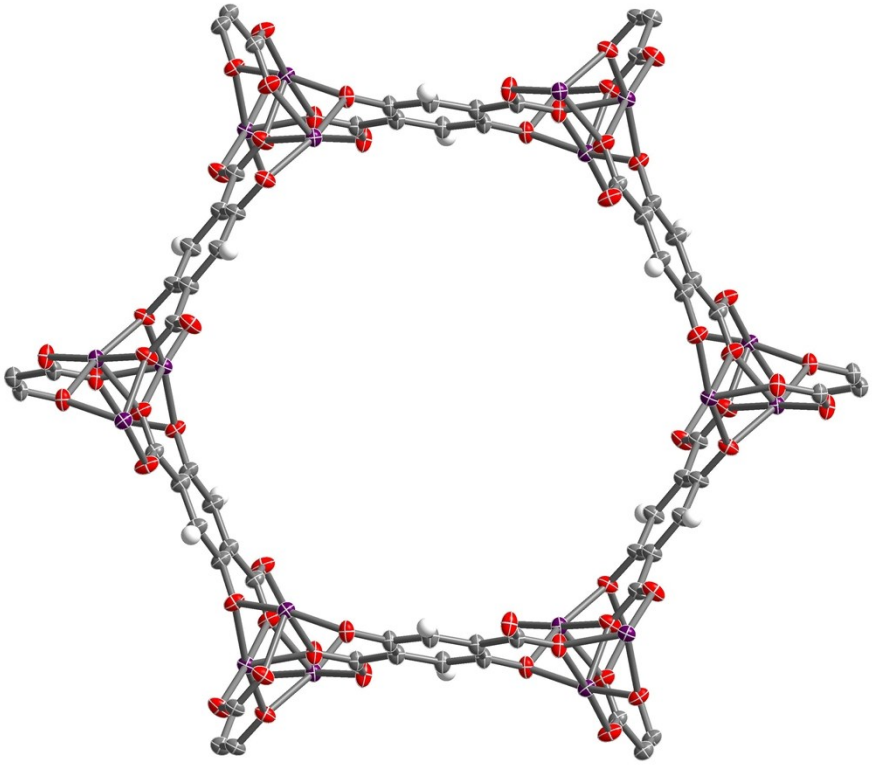

Figure S3. Thermal ellipsoid plot of Co_2(dobdc) at 298 K drawn at 50% probability level as determined by single-crystal X-ray diffraction; purple, red, gray and white ellipsoids represent Co, O, C, and H atoms, respectively.

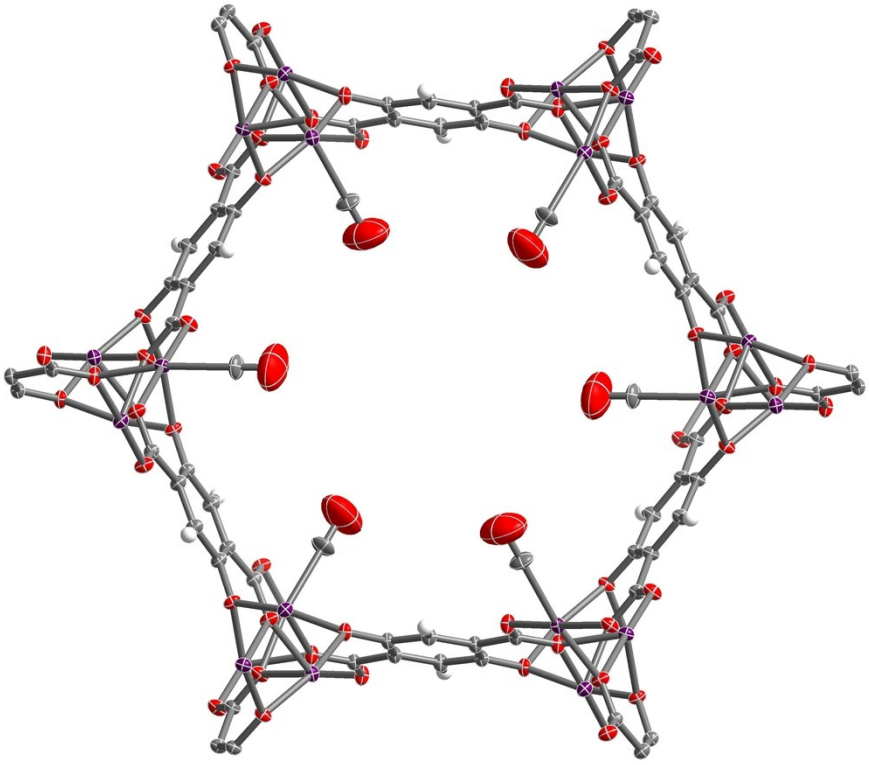

Figure S4. Thermal ellipsoid plot of Co_2(dobdc)·0.58CO at 90 K drawn at 50% probability level as determined by single-crystal X-ray diffraction; purple, red, gray, and white ellipsoids represent Co, O, C, and H atoms, respectively.

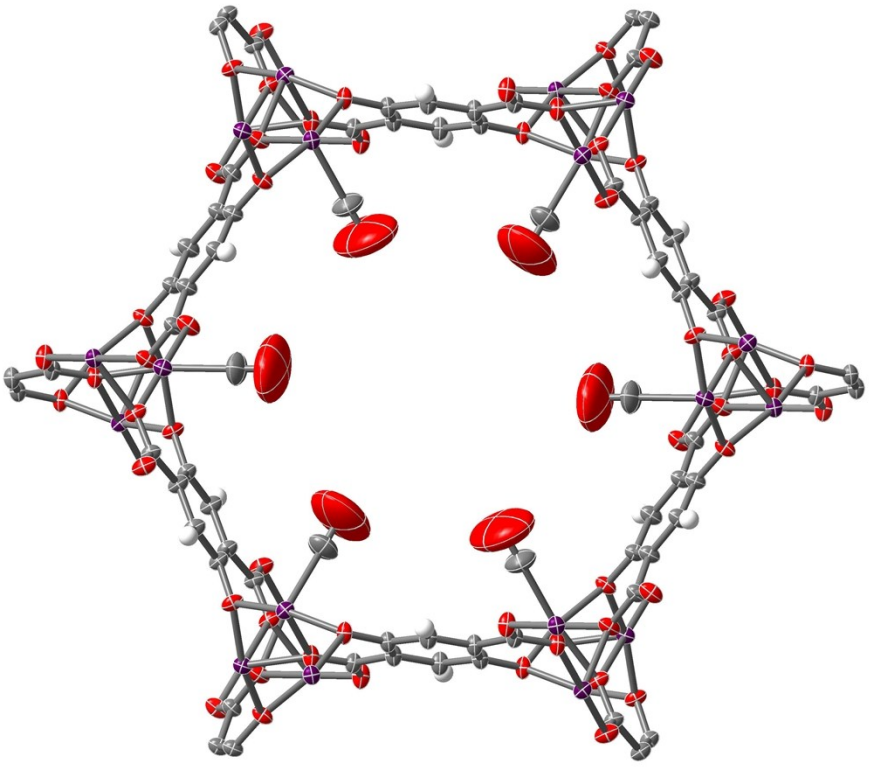

Figure S5. Thermal ellipsoid plot of Co_2(dobdc)·1.2CO at 100 K drawn at 50% probability level as determined by single-crystal X-ray diffraction; purple, red, gray, and white ellipsoids represent Co, O, C, and H atoms, respectively.

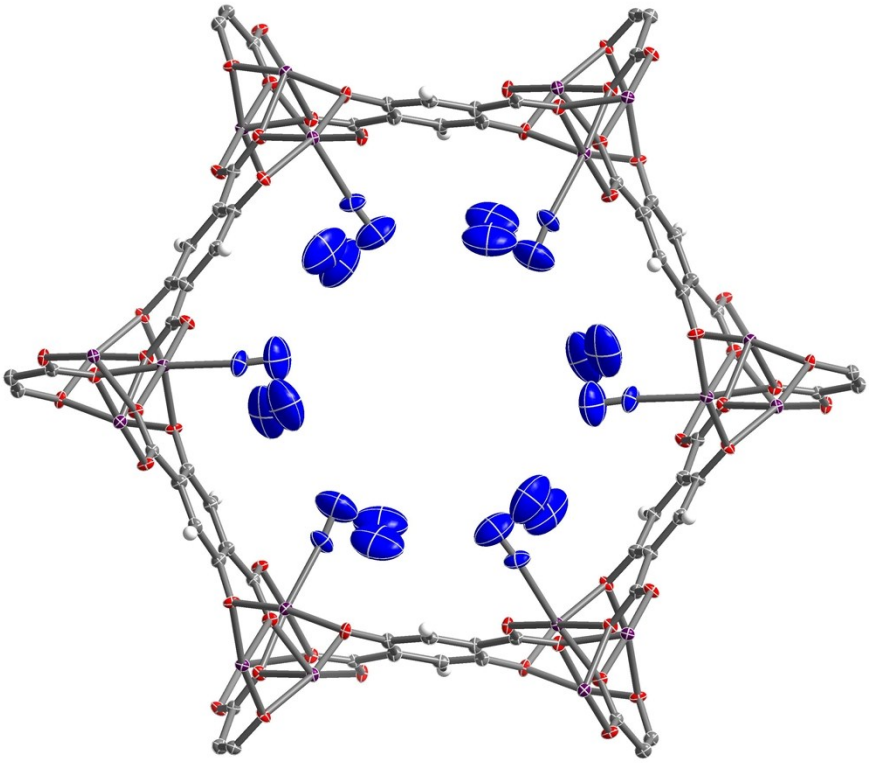

Figure S6. Thermal ellipsoid plot of $Co_2(dobdc)\cdot 3.8N_2$ at 100 K drawn at 50% probability level as determined by single-crystal X-ray diffraction; purple, red, gray, blue, and white ellipsoids represent Co, O, C, N, and H atoms, respectively.

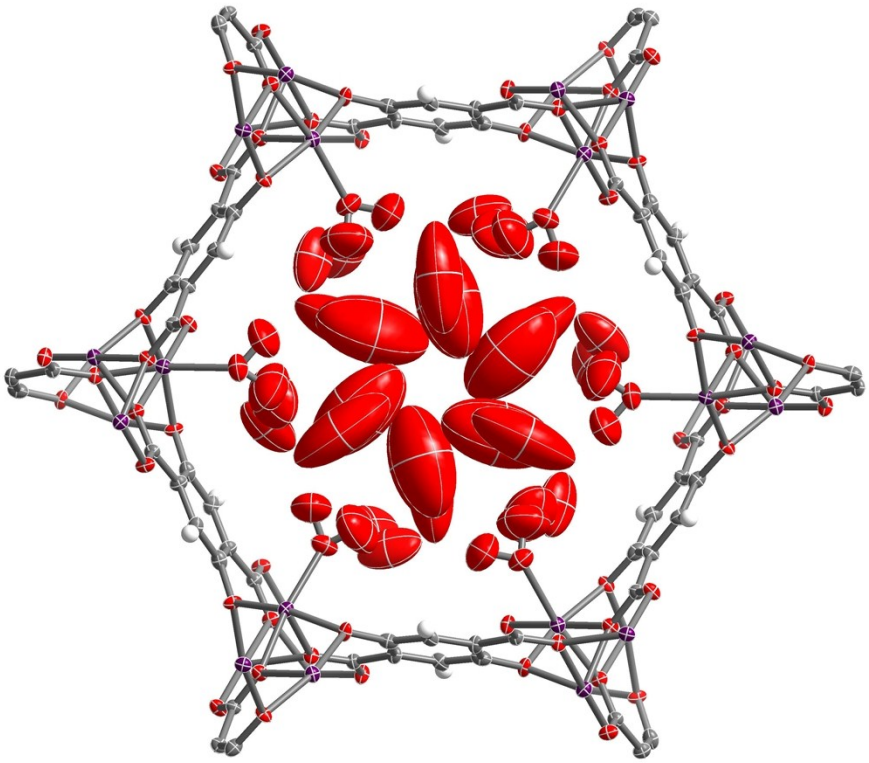

Figure S7. Thermal ellipsoid plot of $Co_2(dobdc)\cdot 5.9O_2$ at 100 K drawn at 50% probability level as determined by single-crystal X-ray diffraction; purple, red, gray, and white ellipsoids represent Co, O, C, and H atoms, respectively. Note, O_2 bound to the Co^{II} sites were found to be disordered over two orientations with relative occupancies of 73(3)% and 27(3)%.

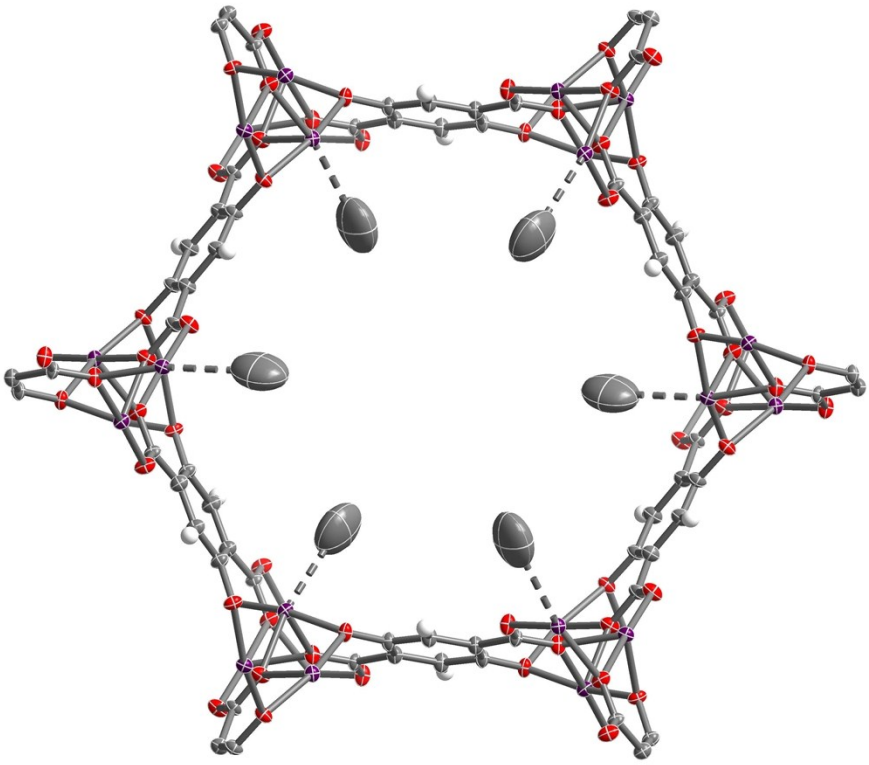

Figure S8. Thermal ellipsoid plot of $Co_2(dobdc)\cdot 2.0CH_4$ at 100 K drawn at 50% probability level as determined by single-crystal X-ray diffraction; purple, red, gray, and white ellipsoids represent Co, O, C, and H atoms, respectively.

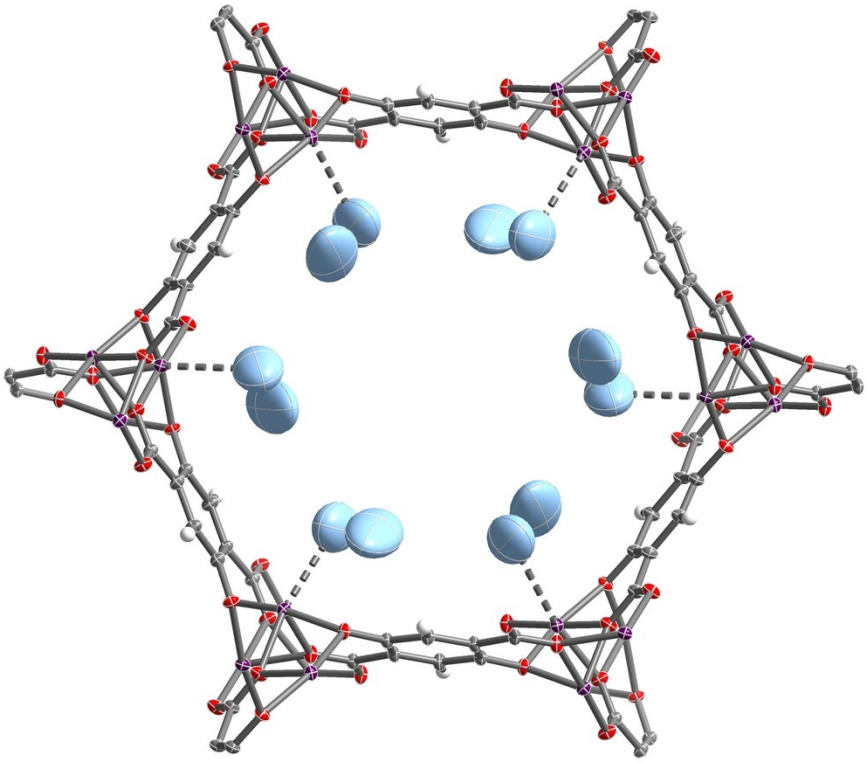

Figure S9. Thermal ellipsoid plot of Co_2(dobdc)·2.0Ar at 90 K drawn at 50% probability level as determined by single-crystal X-ray diffraction; purple, red, gray, light blue, and white ellipsoids represent Co, O, C, Ar, and H atoms, respectively.

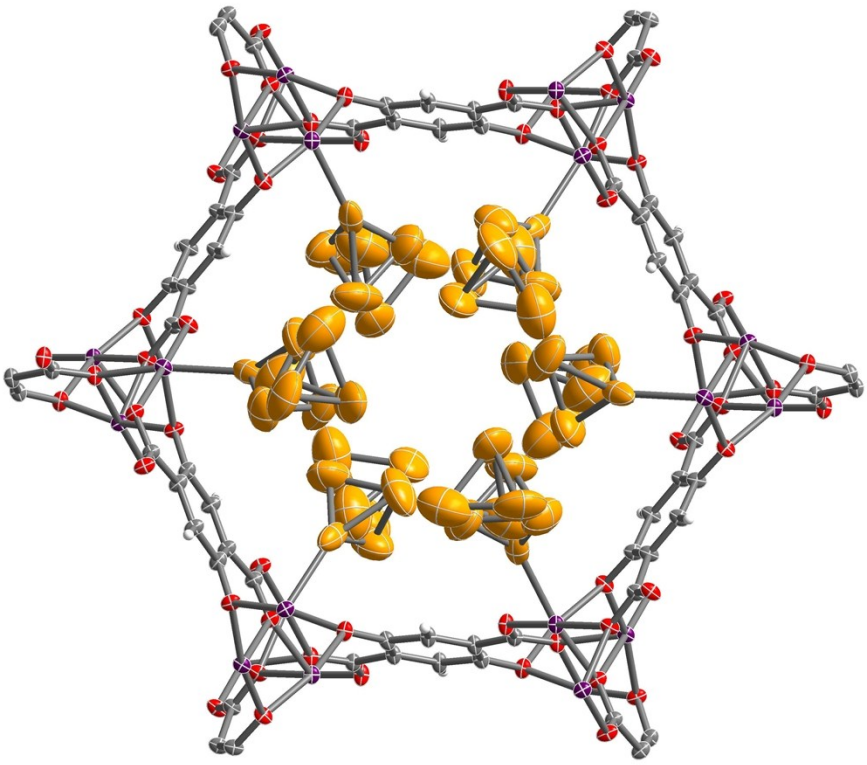

Figure S10. Thermal ellipsoid plot of $Co_2(dobdc)\cdot 1.3P_4$ at 100 K drawn at 50% probability level as determined by single-crystal X-ray diffraction; purple, red, gray, light orange, and white ellipsoids represent Co, O, C, P, and H atoms, respectively. Note, the P_4 molecules were found in two positions, one with P_4 molecules coordinated to the Co^{II} sites (45.5(10)% occupancy) and another 3.88(3) Å away from the Co^{II} sites centers (20.6(10)% occupancy).

Table S1. Crystallographic Data

	Co_2(dobdc)	Co_2(dobdc)·0.58CO	Co_2(dobdc)·1.2CO	Co_2(dobdc)·3.8N_2	Co_2(dobdc)·5.9O_2	Co_2(dobdc)·2.0CH_4	Co_2(dobdc)·2.0Ar	Co_2(dobdc)·1.3P_4
Formula	$Co_2C_8H_2O_6$	$Co_2C_{8.58}H_2O_{6.58}$	$Co_2C_{9.19}H_2O_{7.18}$	$Co_2C_8H_2N_{7.56}O_6$	$Co_2C_8H_2O_{17.88}$	$Co_2C_{10}H_{10}O_6$	$Co_2C_8H_2O_6Ar_2$	$Co_2C_8H_2O_6P_{5.28}$
Temperature (K)	296(2)	90(2)	100(2)	100(2)	100(2)	100(2)	90(2)	100(2)
Crystal System	Trigonal	Trigonal	Trigonal	Trigonal	Trigonal	Trigonal	Trigonal	Trigonal
Space Group	$R\bar{3}$	$R\bar{3}$	$R\bar{3}$	$R\bar{3}$	$R\bar{3}$	$R\bar{3}$	$R\bar{3}$	$R\bar{3}$
a, b, c (Å)	25.892(4), 25.892(4), 6.8482(9)	25.8262(16), 25.8262(16), 6.8315(4)	25.853(3), 25.853(3), 6.8494(7)	25.810(8), 25.810(8), 6.901(2)	25.7599(9), 25.7599(9), 6.8766(3)	25.866(5), 25.866(5), 6.8457(12)	25.860(4), 25.860(4), 6.8678(10)	25.7348(8), 25.7348(8), 6.8385(2)
α, β, γ (°)	90, 90, 120	90, 90, 120	90, 90, 120	90, 90, 120	90, 90, 120	90, 90, 120	90, 90, 120	90, 90, 120
V, (Å^3)	3975.9(12)	3946.1(5)	3964.6(9)	3981(3)	3951.8(3)	3966.4(15)	3977.5(12)	3922.2(3)
Z	9	9	9	9	9	9	9	9
Radiation, λ (Å)	Synchrotron, 0.7749	Synchrotron, 0.7749	Synchrotron, 0.7749	Synchrotron, 0.6199	Synchrotron, 0.7749	Synchrotron, 0.7749	Synchrotron, 0.6525	Synchrotron, 0.7749
2Θ Range for Data Collection (°)	6.782 to 64.176	6.8 to 69.512	6.782 to 69.43	4.768 to 47.466	5.974 to 54.904	6.786 to 65.124	5.696 to 63.570	6.796 to 74.476
Completeness to 2Θ	99.9% (2Θ = 55.412°)	99.0% (2Θ = 55.412°)	99.9% (2Θ = 55.412°)	99.9% (2Θ = 43.670°)	99.1% (2Θ = 54.904°)	99.8% (2Θ = 55.412°)	99.8% (2Θ = 46.096°)	99.9% (2Θ = 55.412°)
Data / Restraints / Parameters	2374 / 0 / 74	2857 / 0 / 92	2885 / 9 / 92	2040 / 8 / 110	1536 / 34 / 138	2442 / 0 / 83	3887 / 6 / 94	3479 / 216 / 148
Goodness of Fit on F^2	1.116	1.070	1.051	1.190	1.015	1.064	1.072	1.198
R1[a], wR2[b] (I>2σ(I))	0.0485, 0.1370	0.0274, 0.0696	0.0389, 0.0978	0.0632, 0.1233	0.0481, 0.1045	0.0477, 0.1205	0.0513, 0.1272	0.0822, 0.2465
R1[a], wR2[b] (all data)	0.0564, 0.1453	0.0317, 0.0718	0.0491, 0.1032	0.0805, 0.1328	0.0860, 0.1203	0.0558, 0.1271	0.0637, 0.1358	0.0902, 0.2530
Largest Diff. Peak and Hole (e Å^{-3})	0.990 and –0.519	0.578 and –0.391	0.454 and –0.432	0.688 and –0.753	0.826 and –0.587	0.777 and –0.482	1.740 and –0.956	2.388 and –1.557

[a] $R_1 = \sum||F_o| - |F_c||/\sum|F_o|$. [b] $wR_2 = \{\sum[w(F_o^2 - F_c^2)^2]/\sum[w(F_o^2)^2]\}^{1/2}$.

Langmuir fits for low-pressure gas adsorption isotherms of Co_2(dobdc)

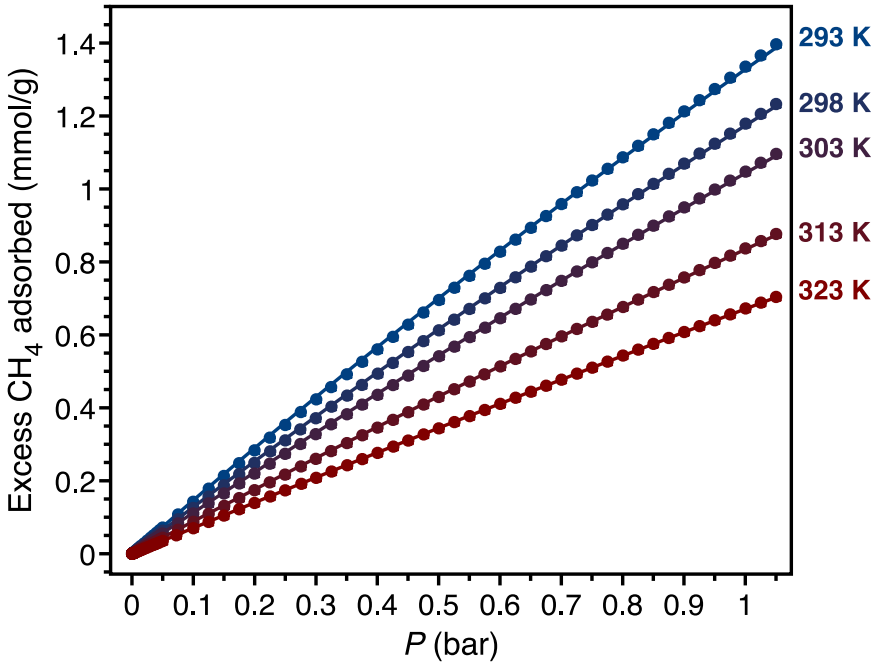

T (K)	$n_{sat,1}$ (mmol/g)	S_1 (R)	$-E_1$ (kJ/mol)	$n_{sat,2}$ (mmol/g)	S_2 (R)	$-E_2$ (kJ/mol)
293.15	6.41	10.6	20.6	6.41	9.39	17.6
298.15	6.41	10.5	20.3	6.41	9.33	17.4
303.15	6.41	10.6	20.6	6.41	9.42	17.6
313.15	6.41	10.6	20.6	6.41	9.42	17.6
323.15	6.41	10.5	20.4	6.41	9.39	17.5

Figure S11. Dual-site Langmuir fits and parameters for CH_4 adsorption isotherms of Co_2(dobdc) at 293.15, 298.15, 303.15, 313.15, 323.15 K (fit independently for each temperature); T is the temperature, $n_{sat,1}$ is the saturation capacity, S_i is the site-specific molar entropy of adsorption, E_i is the site-specific binding energy, and R is the gas constant in J/mol·K.

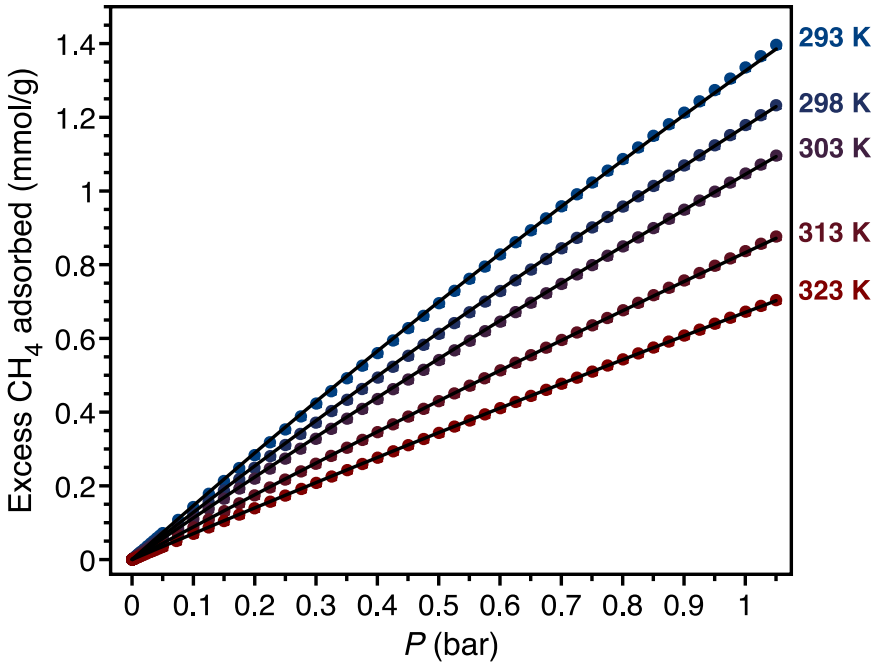

$n_{sat,1}$ (mmol/g)	S_1 (R)	$-E_1$ (kJ/mol)	$n_{sat,2}$ (mmol/g)	S_2 (R)	$-E_2$ (kJ/mol)
6.41	10.1	19.4	6.41	10.1	19.3

Figure S12. Dual-site Langmuir fits and parameters for CH_4 adsorption isotherms of Co_2(dobdc) at 293.15, 298.15, 303.15, 313.15, 323.15 K (fit simultaneously for all temperatures); $n_{sat,I}$ is the saturation capacity, S_i is the site-specific molar entropy of adsorption, E_i is the site-specific binding energy, and R is the gas constant in J/mol·K.

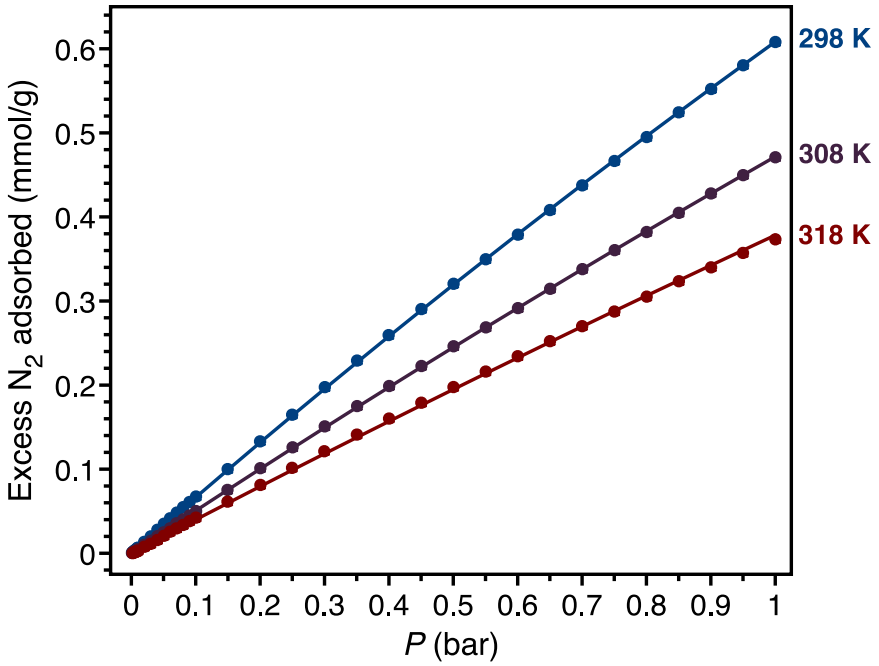

T (K)	$n_{sat,1}$ (mmol/g)	S_1 (R)	$-E_1$ (kJ/mol)
298.15	6.41	10.1	19.5
308.15	6.41	10.2	19.6
318.15	6.41	10.2	19.6

Figure S13. Single-site Langmuir fits and parameters for N_2 adsorption isotherms of Co_2(dobdc) at 298.15, 308.15, and 318.15 K (fit independently for each temperature); T is the temperature, $n_{sat,1}$ is the saturation capacity, S_i is the site-specific molar entropy of adsorption, E_i is the site-specific binding energy, and R is the gas constant in J/mol·K.

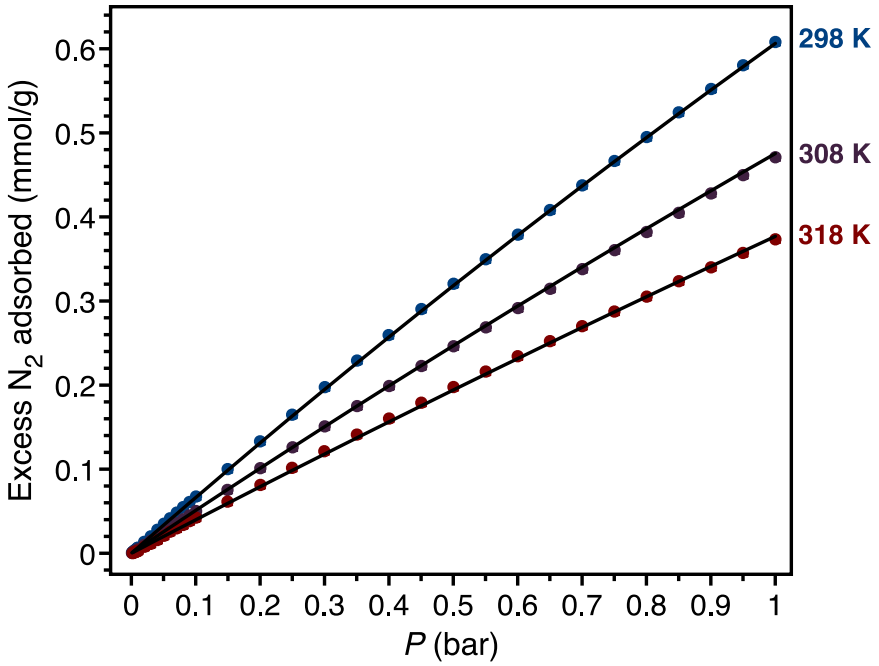

$n_{sat,1}$ (mmol/g)	S_1 (R)	$-E_1$ (kJ/mol)
6.41	10.4	20.3

Figure S14. Single-site Langmuir fit and parameters for N_2 adsorption isotherms of Co_2(dobdc) at 298.15, 308.15, and 318.15 K (fit simultaneously for all temperatures); $n_{sat,1}$ is the saturation capacity, S_i is the site-specific molar entropy of adsorption, E_i is the site-specific binding energy, and R is the gas constant in J/mol·K.

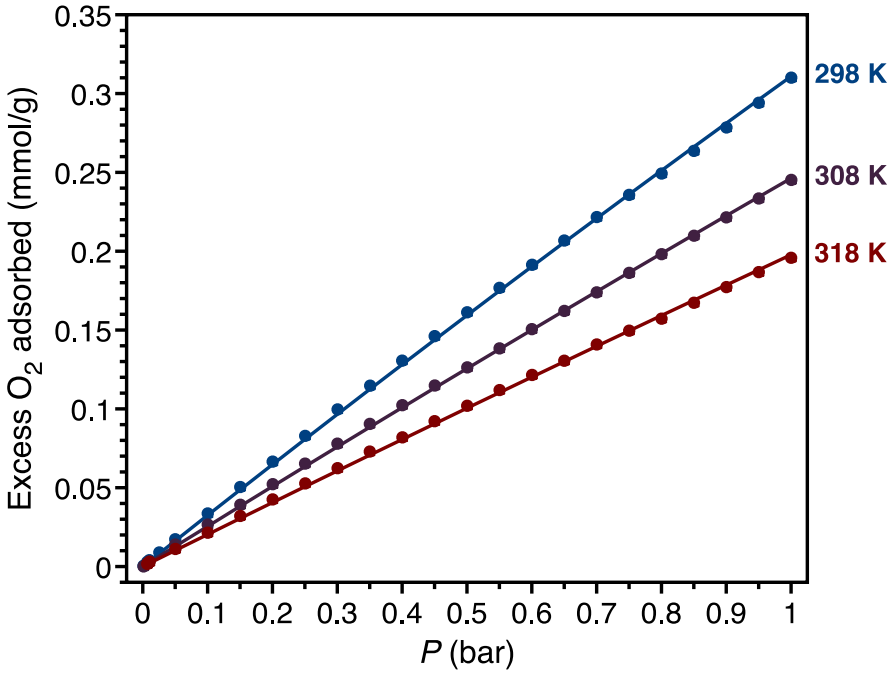

T (K)	$n_{sat,1}$ (mmol/g)	S_1 (R)	$-E_1$ (kJ/mol)
298.15	6.41	10.6	18.8
308.15	6.41	10.6	19.0
318.15	6.41	10.6	19.0

Figure S15. Single-site Langmuir fits and parameters for O_2 adsorption isotherms of Co_2(dobdc) at 298.15, 308.15, and 318.15 K (fit independently for each temperature); T is the temperature, $n_{sat,1}$ is the saturation capacity, S_i is the site-specific molar entropy of adsorption, E_i is the site-specific binding energy, and R is the gas constant in J/mol·K.

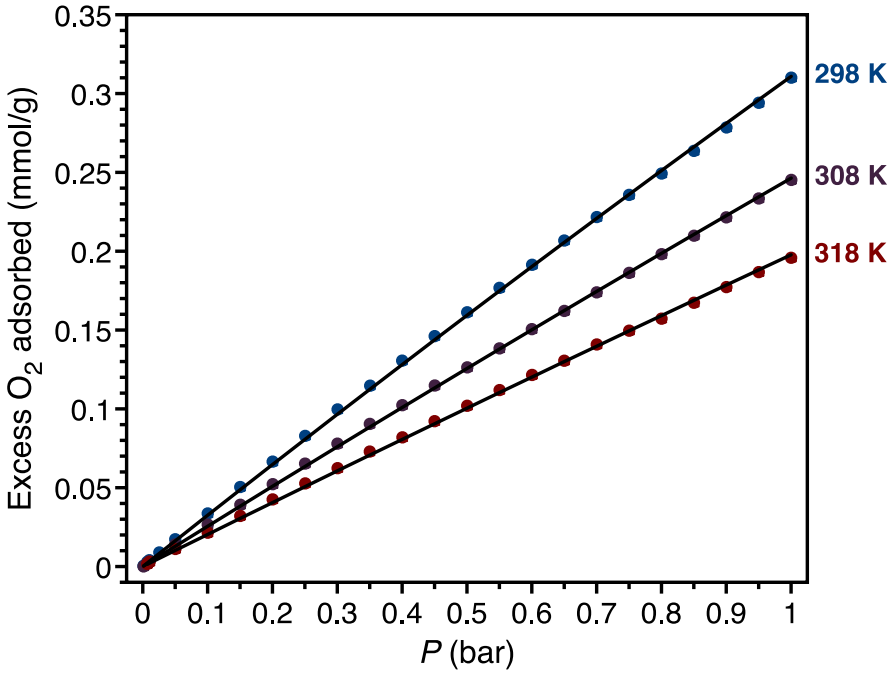

$n_{sat,1}$ (mmol/g)	S_1 (R)	$-E_1$ (kJ/mol)
6.41	10.5	18.5

Figure S16. Single-site Langmuir fits and parameters for O_2 adsorption isotherms of Co_2(dobdc) at 298.15, 308.15, and 318.15 K (fit simultaneously for all temperatures); $n_{sat,1}$ is the saturation capacity, S_i is the site-specific molar entropy of adsorption, E_i is the site-specific binding energy, and R is the gas constant in J/mol·K.

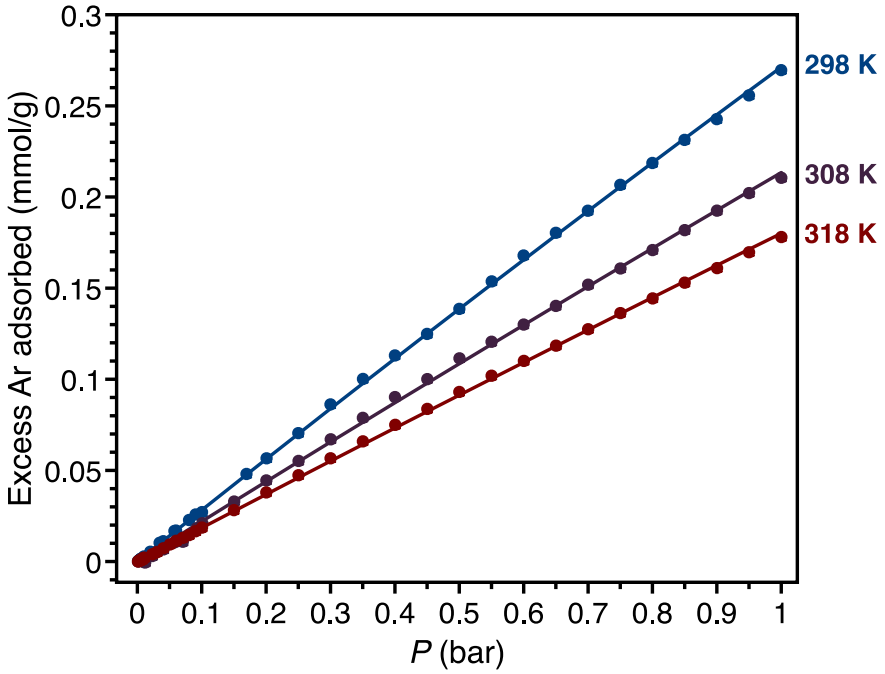

T (K)	$n_{sat,1}$ (mmol/g)	S_1 (R)	$-E_1$ (kJ/mol)
298.15	6.41	9.88	16.8
308.15	6.41	9.90	16.7
318.15	6.41	9.82	16.6

Figure S17. Single-site Langmuir fits and parameters for Ar adsorption isotherms of Co_2(dobdc) at 298.15, 308.15, and 318.15 K (fit independently for each temperature); T is the temperature, $n_{sat,1}$ is the saturation capacity, S_i is the site-specific molar entropy of adsorption, E_i is the site-specific binding energy, and R is the gas constant in J/mol·K.

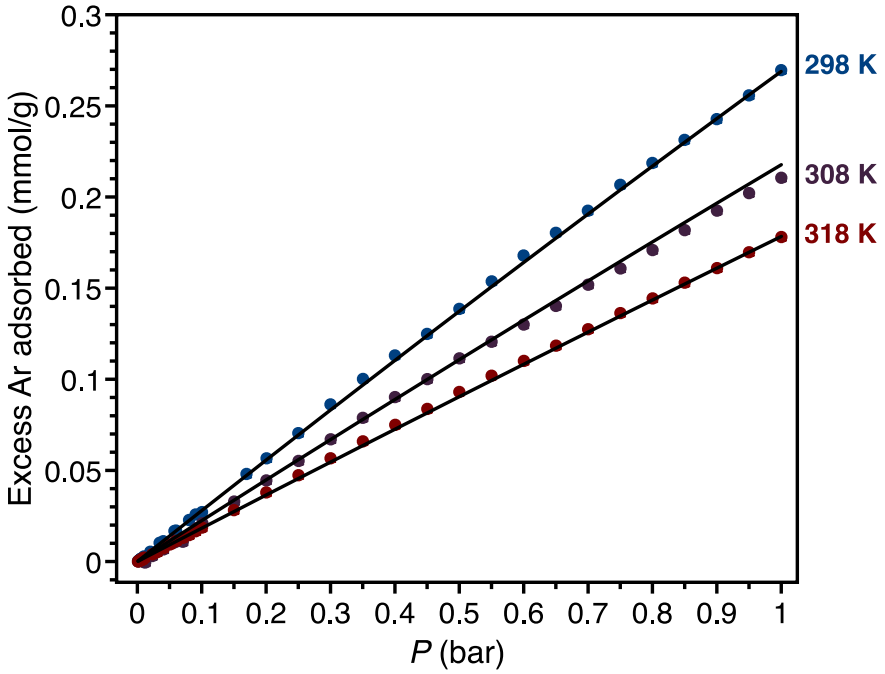

$n_{sat,1}$ (mmol/g)	S_1 (R)	$-E_1$ (kJ/mol)
6.41	9.89	16.7

Figure S18. Single-site Langmuir fits and parameters for Ar adsorption isotherms of Co_2(dobdc) at 298.15, 308.15, and 318.15 K (fit simultaneously for all temperatures); $n_{sat,1}$ is the saturation capacity, S_i is the site-specific molar entropy of adsorption, E_i is the site-specific binding energy, and R is the gas constant in J/mol·K.

Low-coverage differential enthalpy of adsorption plots for Co_2(dobdc)

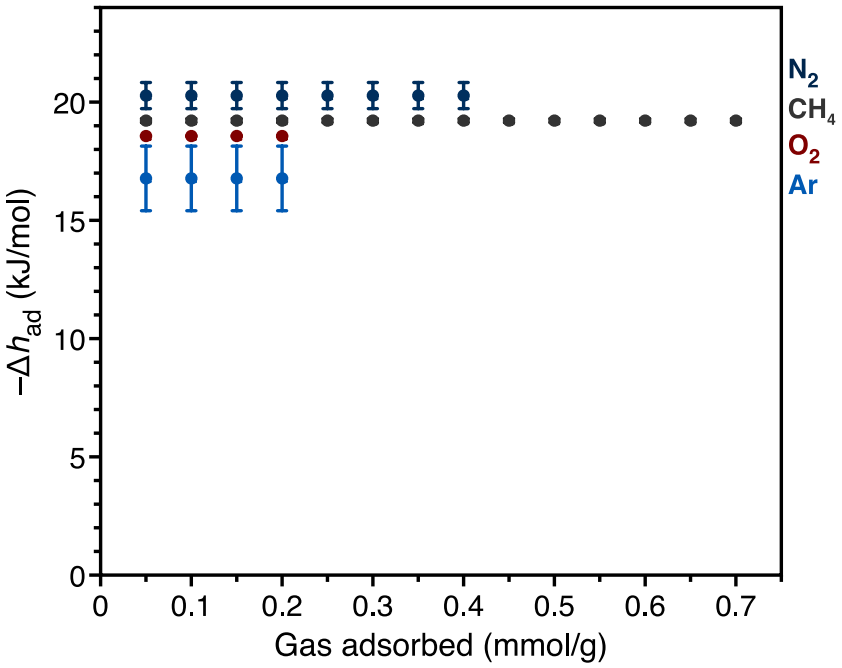

Figure S19. Low-coverage differential enthalpy of adsorption (Δh_{ad}) plots (calculated using independent Langmuir fits to low-pressure adsorption isotherms) for CH_4 (gray), N_2 (dark blue), O_2 (red), and Ar (light blue) adsorption in Co_2(dobdc). Error bars for CH_4 and O_2 are smaller than the symbols used for the data.

References

1 W. L. Queen, M. R. Hudson, E. D. Bloch, J. A. Mason, M. I. Gonzalez, J. S. Lee, D. Gygi, J. D. Howe, K. Lee, T. A. Darwish, M. James, V. K. Peterson, S. J. Teat, B. Smit, J. B. Neaton, J. R. Long and C. M. Brown, *Chem. Sci.*, 2014, **5**, 4569–4581.

2 R. Mercado, B. Vlaisavljevich, L.-C. Lin, K. Lee, Y. Lee, J. A. Mason, D. J. Xiao, M. I. Gonzalez, M. T. Kapelewski, J. B. Neaton and B. Smit, *J. Phys. Chem. C*, 2016, **120**, 12590–12604.